

# YIG Photonic Crystals

A. Rashedi,<sup>1</sup> M. Ebrahimi,<sup>1</sup> Y. Huang,<sup>1</sup> M. J. Rudd,<sup>1</sup> and J.P. Davis<sup>1</sup>  
*Department of Physics, University of Alberta, Edmonton, Alberta T6G 2E9, Canada<sup>a)</sup>*

(Dated: 10 December 2024)

We present the first demonstration of a nanofabricated photonic crystal made from the magnetic material yttrium iron garnet (YIG). YIG is a compelling material for quantum technologies due to its unique magnetic and optical properties; however, experiments involving YIG have primarily been limited to millimeter-scale spheres. The successful nanofabrication of YIG structures opens new avenues for advancing quantum technology applications. Notably, the ability to co-localize magnons, phonons, and optical photons within a nanostructured environment paves the way for novel approaches in quantum information processing, including quantum wavelength transduction and enhanced magnon-photon interactions. This work marks a significant step toward integrating YIG-based devices into scalable quantum platforms.

Hybrid quantum systems are emerging as a promising pathway in the advancement of quantum technologies. By integrating the strengths of individual systems while mitigating their weaknesses, these platforms offer enhanced capabilities and functionalities. Optomechanical and magnomechanical platforms are prime examples of such systems. Optomechanical systems<sup>1–3</sup>, in particular, combine optical and mechanical resonators to perform a variety of tasks, ranging from dark matter detection<sup>4–8</sup> to ultra-sensitive torque and magnetic measurements<sup>9–11</sup>, as well as coherent transduction of microwave photons to optical photons<sup>12–17</sup> and numerous other applications<sup>18–22</sup>. These systems can offer similar functionality, but with a smaller footprint, when compared to other platforms such as atomic vapors<sup>23,24</sup>.

An important class within optomechanical systems is the optomechanical crystal cavity (OMC)<sup>25–29</sup>. These structures consist of photonic and phononic crystal cavities that simultaneously confine optical and mechanical modes within a small volume. Such nanostructures are incredibly versatile and can be precisely engineered for specific applications, enhancing the interaction between light and mechanical vibrations. This strong coupling is significant for quantum information processing, precision sensing, and other quantum technologies. Optomechanical crystals have been realized in various materials, including silicon, silicon nitride, gallium arsenide, and diamond<sup>14,25,30–32</sup>.

Magnomechanical systems, another type of hybrid system, focus on interactions between magnons—the quanta of spin waves—and phonons<sup>33</sup>. Yttrium iron garnet (YIG) is the preferred material for magnonic systems<sup>34</sup> due to its exceptionally low Gilbert damping<sup>35</sup> ( $\alpha \approx 10^{-5}$ ) and low optical absorption in the infrared region<sup>36</sup>. YIG macroscopic spheres have been extensively studied<sup>37–44</sup>. However, the inadequate mode overlap between phononic and magnonic modes in YIG spheres limits the single phonon-magnon coupling rate to the millihertz range, preventing the achievement of strong coupling. To overcome this limitation, there is a need for nano- and microfabrication of YIG structures to enhance mode overlap.

Realizing an optomechanical crystal cavity in a magnetic

material like YIG promises to bridge the gap between optomechanical and magnomechanical systems. This integration would enable the creation of a multiparticle system capable of addressing various contemporary challenges, such as achieving near-unity efficiency in the coherent conversion of microwave photons to telecommunication photons<sup>45,46</sup>.

One primary challenge to such a platform is that YIG is not compatible with the conventional fabrication methods used for other materials hosting optomechanical crystals, such as silicon and silicon nitride. Despite significant efforts toward fabricating micro- and nanostructures in YIG, these attempts have resulted in relatively simple geometries that cannot support optical photons<sup>47–52</sup>. To date, no nanostructure has been achieved that can host optical photons, phonons, and magnons simultaneously in a microvolume.

In this work, we present the first observation of optical resonance in a nanofabricated optomechanical crystal cavity made from YIG, designed to support three types of bosonic quasiparticles: optical photons, phonons, and magnons. This structure enables interactions between these quasiparticles by confining them within a shared volume and increasing their mode overlap. Our work lays the foundation for functional optomagnomechanical devices.

## I. DESIGN AND FABRICATION

To realize a platform that hosts optical, mechanical, and magnon modes simultaneously, we began by designing an OMC similar to the diamond OMC of Burek et al.<sup>32</sup>. The device consists of a suspended rectangular YIG nanobeam patterned along its length by elliptical holes of varying dimensions, forming a photonic crystal waveguide. It is doubly clamped by the YIG substrate at both ends, as shown in Fig. 1(a)–(c) and Fig. 2(f). We optimized the optical bandgap of the device via finite element method (FEM) simulations in COMSOL Multiphysics<sup>53</sup> to confine an optical mode at  $\omega_0/2\pi \approx 187$  THz ( $\sim 1600$  nm), depicted by the cyan horizontal dashed line deep within the optical bandgap, as shown in Fig. 1(d).

Modes with most of their electric field perpendicular to the beam axis (TE-like) are shown with solid blue lines, and modes with most of their electric field parallel to the beam axis

<sup>a)</sup>Electronic mail: jdavis@ualberta.ca

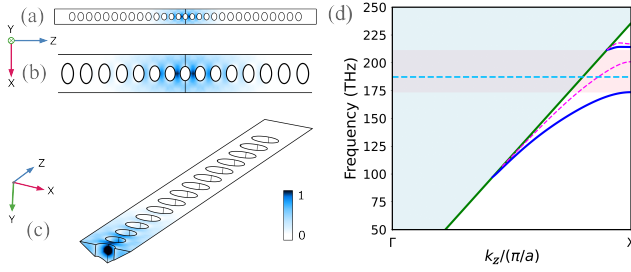


FIG. 1: Design of the YIG optomechanical crystal cavity (OMC). (a)-(c) Amplitude profile of the confined optical mode's electric field, illustrating that most of the field is concentrated in the center of the beam and within the YIG, which is essential for achieving a high phonon-photon-magnon coupling rate. (b) A zoomed view of the cavity area of the waveguide. (c) A cross-sectional view of the center of the waveguide. (d) Optical band diagram of the OMC, where the solid blue lines represent the guided transverse electric (TE-like) modes, and the dashed magenta lines depict the guided transverse magnetic (TM-like) modes of the waveguide. The shaded pink region indicates the optical semi-band gap, intersected by the light line (green solid line), while the continuous leaky modes coupling to air are represented by the shaded blue area above the light line. The confined mode at the edge of the first Brillouin zone is highlighted by the cyan horizontal dashed line.

(TM-like) are shown with dashed magenta lines in Fig. 1(d). Due to symmetry and polarization mismatch, TE-like and TM-like modes do not couple to one another, enabling a large bandgap of 40 THz for TE-like modes. The electric field amplitude profile of the confined optical mode at the edge of the first Brillouin zone is shown in Fig. 1(a)-(c).

As previously mentioned, YIG does not yet have standardized processes compatible with conventional microfabrication techniques. Therefore, we turn to focused ion beam (FIB) milling, which uses high-energy ion beams to physically remove material, sculpting the final design from the substrate—effectively functioning as a nano-scale computer numerical control (CNC) machine<sup>54</sup>. The high-energy nature of the ion beam introduces several challenges that can degrade the quality of the final structure. During the milling process, issues such as heat generation, ion implantation, and re-deposition of sputtered material can significantly affect the precision and functionality of the final device.

The localized heating from the ion beam can alter the material properties of YIG or cause structural deformation, impacting the device's functionality. Additionally, ion implantation, where some ions from the beam embed into the YIG substrate, can modify its magnetic or optical properties, potentially introducing defects<sup>55–57</sup>. Furthermore, material redeposition, in which removed material settles onto unwanted areas, can lead to excess surface roughness and otherwise contaminate high-precision regions.

Our substrate consists of an 840 nm thick layer of YIG with a (111) crystallographic orientation on a 500  $\mu\text{m}$  thick gadolinium gallium garnet (GGG) base. To mitigate the issues associated with FIB milling, we introduce a sacrificial aluminum layer deposited on the YIG surface at the outset. Aluminum was chosen for several reasons. First, it is com-

monly used as a hard mask in Si and SiN fabrication and can be easily removed using standard wet etching processes. Second, aluminum effectively conducts heat, aiding in heat dissipation and thereby reducing the risk of heat-induced damage to the YIG substrate. Third, during the milling process, any redeposited material settles on this sacrificial layer, which can then be easily removed along with the Al layer, ensuring a cleaner final structure. Finally, this aluminum layer serves as a barrier, reducing the implantation of FIB ions into the substrate and preserving the integrity of the YIG layer.

After sputtering the aluminum layer onto the YIG substrate, we milled two trenches to form a bridge structure, as shown in Fig. 2(b). This initial milling creates the general outline of the device. Next, we carefully rotate the sample by 40 degrees to allow for an angled undercut of the bridge, forming a suspended triangular beam that will serve as the base of the waveguide, as illustrated in Fig. 2(c). Following this, we switch to lower ion beam currents to finely trim and shape the

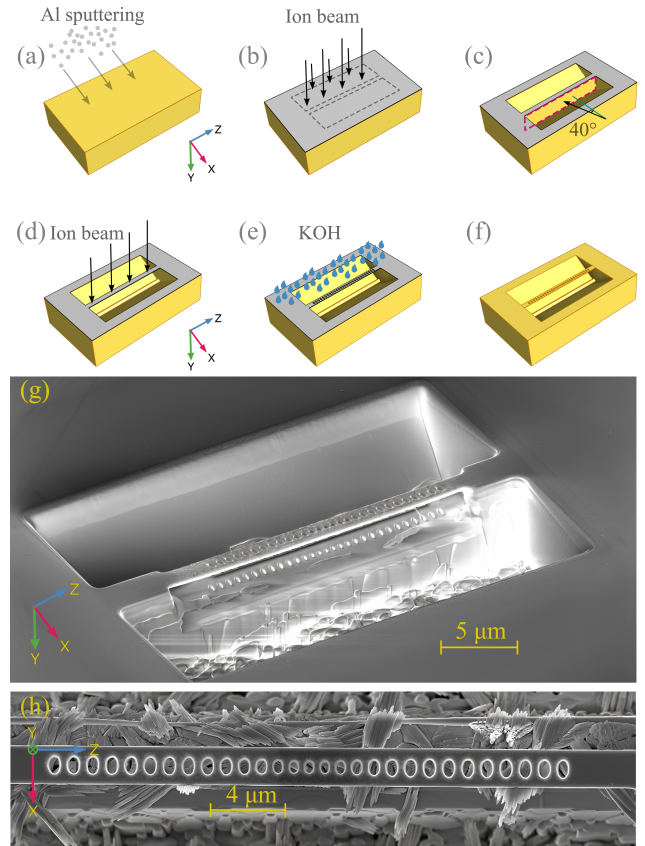


FIG. 2: (a)-(f) Fabrication process flow of the YIG optomechanical crystal cavity (OMC). (a) The process begins with the deposition of a sacrificial aluminum (Al) layer on the YIG substrate. (b)-(d) The ion beam is then used to mill the trenches, shape the beam, and precisely drill the elliptical holes. (e) The final step involves removing the Al layer using a potassium hydroxide (KOH) wet etch to reveal the completed YIG OMC. (f) The result is a suspended structure ready for characterization. (g) Scanning electron micrograph (SEM) of the prepared device before the Al removal step. (h) SEM of the finished device.

beam down to its final dimensions: a width of  $1.25\ \mu\text{m}$  and a length of  $20\ \mu\text{m}$ . This reduction in current helps achieve greater precision, preventing unnecessary material removal and minimizing heat-related deformation. Once the beam has been trimmed, we return the sample to the default position (zero angle) and use a low-current ion beam to carefully drill the elliptical holes required for the design. These holes play a crucial role in defining the optical, mechanical and magnonic properties of the waveguide, so this step requires meticulous control to ensure their placement and size are accurate. The final step in the process involves removing the sacrificial aluminum layer using a potassium hydroxide (KOH) bath. This step is critical, as it not only removes any residual aluminum but also leaves the YIG structure clean and free from contaminants. Finally, we dry the chip using a critical point drying technique<sup>58</sup> to avoid any damage from water surface tension forces, preserving the suspended structure.

## II. OPTICAL CHARACTERIZATION

The optical characterization setup is relatively straightforward. A tunable laser diode source directs light into an optical fiber polarization controller. The light is then guided into a tapered, dimpled optical fiber<sup>59</sup>, where the evanescent field of the dimpled region overlaps with the confined TE-like

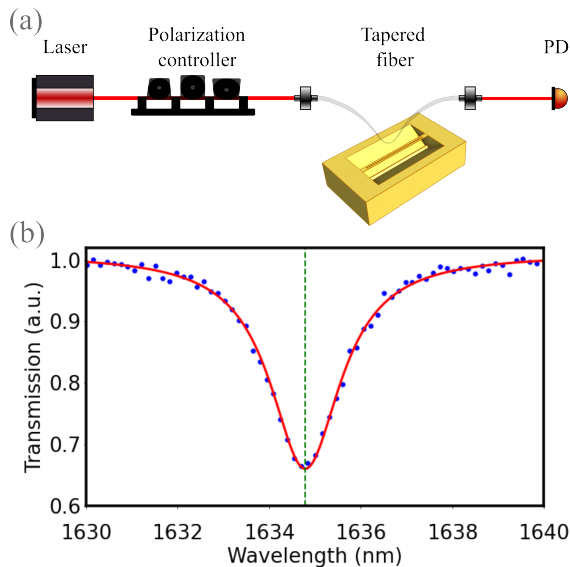


FIG. 3: (a) Schematic of the optical characterization setup. The setup utilizes a Santec TSL570 tunable laser source, with light from this source passing through a polarization controller to maximize coupling efficiency between the tapered dimpled fiber and the device. The transmitted signal is then detected by a Resolved Instruments DPD80 photodetector and analyzed. (b) The transmission spectrum reveals a resonance at  $\lambda = 1634.8\ \text{nm}$ . By fitting a Lorentzian function to the data, we extract an internal quality factor of 2000 and an external coupling rate of  $\kappa = 9\ \text{GHz}$ . The red solid line represents the Lorentzian fit, while the blue dots show the experimental data points.

mode's field, enabling light coupling into and out of the device (Fig. 3(a)). The light collected from the device by the dimpled fiber is detected by a Resolved Instruments 80 MHz photodetector and transmitted by USB to a computer for analysis.

The room temperature transmission spectrum of the OMC shows a resonance at  $\lambda = 1634.8\ \text{nm}$  with an internal quality factor of 2000 (Fig. 3(b)), which is considerably lower than its simulated value of  $10^6$ . This discrepancy is attributed to surface roughness and fabrication imperfections, which can be addressed by optimizing the device geometry for FIB fabrication and will be addressed in the next generation of devices. This low internal quality factor (Q) places the device in the unresolved sideband regime<sup>1</sup>, defined by  $\kappa \gg \Omega_m$ , where  $\Omega_m$  is the mechanical mode frequency and  $\kappa$  is the optical mode decay rate. In this regime, the interaction between optical and mechanical modes is significantly weaker, complicating the detection and measurement of the mechanical mode<sup>60</sup>. Owing to these higher-than-anticipated optical losses, we experienced significant challenges resolving the mechanical spectrum of our device and we do not present such measurements in this work. Overcoming these challenges requires further refinement of our fabrication process to achieve higher optical quality factors and to move the device into the sideband-resolved regime for future studies.

## III. PHONONIC AND MAGNONIC MODES

### A. Phononic mode

We designed our photonic crystal with mechanical and magnon modes in mind, allowing the waveguide to function as a photonic, phononic and magnonic waveguide, featuring overlapping guided photonic and phononic modes. The mechanical band diagram, shown in Fig. 4(b), highlights a pink-shaded bandgap region. Similar to the photonic case, the phononic waveguide confines an  $x$ -symmetric phononic mode at  $\Omega_m/2\pi \approx 1.52\ \text{GHz}$  within this mechanical bandgap (Fig. 4(b)). The mode profile and regions of maximum strain are illustrated in Fig. 4(a), demonstrating the mode's potential for strong interactions with the photonic mode via radiation pressure.

To achieve this design, we conducted a series of finite element method (FEM) simulations in COMSOL Multiphysics to maximize the bandgaps and optimize both the optical and mechanical quality factors simultaneously<sup>61</sup>. Once the photonic and phononic modes were identified, we calculated the anticipated single photon- single phonon coupling rate,  $g_0$ <sup>61</sup>, to be 50 kHz. While this value is low compared to counterparts fabricated in materials such as silicon and silicon nitride, it is attributed to YIG's relatively lower photoelastic tensor values<sup>62,63</sup>. These values contribute to a reduced photoelastic coupling term, resulting in an order-of-magnitude decrease in coupling strength for our YIG OMC when compared to silicon-based devices<sup>28,61,64</sup>.

To address this limitation, future iterations of the device will focus on a design where the moving boundary effect is

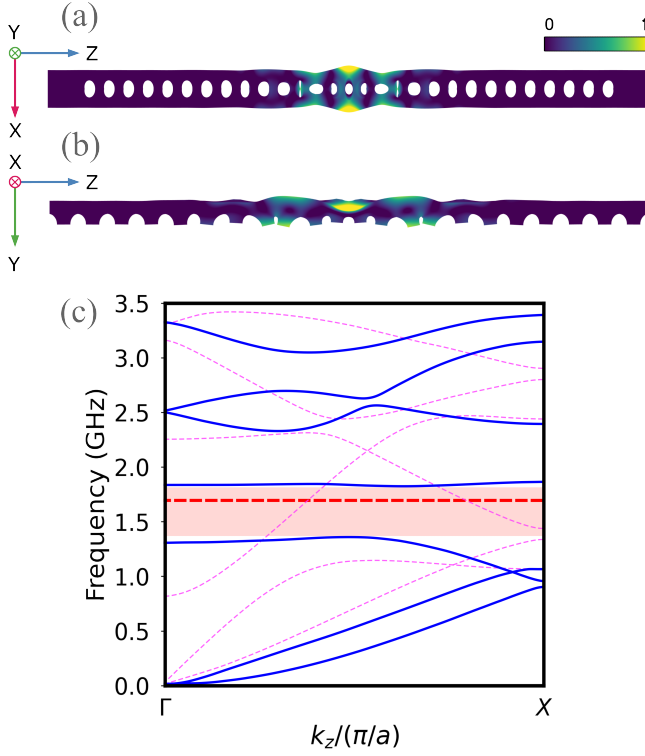


FIG. 4: (a),(b) Displacement field of the mechanical mode (not to scale) at  $\Omega_m/2\pi \approx 1.52$  GHz. (c) Mechanical band diagram of the phononic waveguide. The  $x$ -symmetric and  $x$ -antisymmetric modes are represented by solid blue lines and dashed magenta lines, respectively. The bandgap formed by the  $x$ -symmetric modes is shaded in pink, with the supported confined mode indicated by the red horizontal dashed line.

the dominant coupling mechanism<sup>64</sup>, as seen in ‘zipper’ and slot-mode optomechanical cavities<sup>65–67</sup>. This approach is expected to enhance the coupling efficiency by taking advantage of structural motion more effectively than the current design.

## B. Magnonic mode

In addition to supporting photonic and phononic modes, our optomechanical crystal design facilitates the confinement and manipulation of magnonic modes within YIG. Similar to how photonic crystals control the propagation of light, magnonic crystals enable control over spin wave dynamics by introducing periodic variations in magnetic properties<sup>68</sup>. By applying a strong external magnetic field, we align the magnetization in a specific direction, allowing for precise investigation of spin wave modes in our nanostructure.

Given the micrometer scale of our device, dipolar spin waves are the primary focus of our study<sup>68</sup>. These spin waves are characterized based on their propagation direction relative to the magnetization vector  $\vec{M}_0$  and the external magnetic field  $\vec{H}_{\text{ext}}$ . In our configuration, where the external magnetic field is applied in-plane along the  $z$ -axis, we excite backward volume spin waves, which are well-suited for our experimental

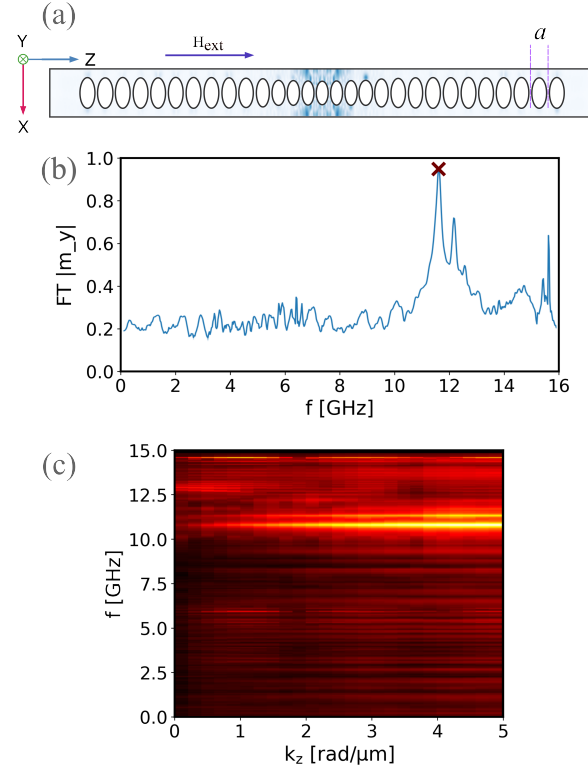


FIG. 5: Magnonic mode simulations. (a) Spatial profile of the  $y$ -component of the reduced magnetization ( $|m_y|$ ) at  $\omega_{\text{mag}} = 11.59$  GHz, showing the confined magnonic mode within the structure. (b) Mode spectrum at the edge of the Brillouin zone ( $k_z = \pi/a$ , where  $a = 650$  nm is the lattice constant), indicating the presence of the localized mode. (c) Band diagram of the backward volume waves within the Brillouin zone, illustrating the propagation characteristics of the spin waves in the magnonic crystal.

objectives<sup>69</sup>.

To simulate the magnonic modes in our structure, we employ the finite-difference simulation tool MuMax3<sup>70</sup>, which numerically solves the Landau-Lifshitz-Gilbert (LLG) equation for the local magnetization dynamics. We use material parameters specific to YIG: a saturation magnetization  $M_s = 140$  kA/m, an exchange stiffness constant  $A_{\text{ex}} = 2$  pJ/m, and a cubic anisotropy constant  $K_c = -610$  J/m<sup>3</sup>, with the anisotropy axis aligned along the  $y$ -axis<sup>57</sup>. The external magnetic field is set to  $H_{\text{ext}} = 400$  mT.

Our simulations reveal that the magnonic crystal structure effectively confines specific magnonic modes within the device (Fig. 5). A localized magnonic mode is observed at a frequency of  $\omega_{\text{mag}} = 2\pi \times 11.59$  GHz. This confinement results from the periodic geometry of the structure and the in-plane applied magnetic field, which together tailor the spin wave dynamics to support backward volume waves.

Figure 5(a) shows the spatial profile of the reduced magnetization’s  $y$ -component ( $|m_y|$ , where  $\vec{m} = \vec{M}/M_s$  with  $M_s$  representing the saturation magnetization) for the confined magnonic mode. The highest intensity is concentrated in the central region of the device, demonstrating spatial localization. The band structure of the backward volume waves across

the Brillouin zone is presented in Fig. 5(c), illustrating the propagation of these waves within the crystal lattice.

By integrating magnonic modes into our optomechanical crystal cavity, we enhance the potential for strong interactions between magnons, phonons, and photons within the same microvolume.

#### IV. CONCLUSION

We have demonstrated the first nanofabricated optomechanical crystal cavity made from yttrium iron garnet, successfully observing the optical resonance at a wavelength of  $\lambda = 1634.8\text{nm}$  with an internal quality factor of approximately 2000. This device is designed to simultaneously host optical photons, phonons, and magnons. This achievement represents a significant advancement in hybrid quantum systems, enabling the co-localization and interaction of all three of the above quasiparticles within a shared nanoscale volume. It opens new avenues for quantum information processing and networking applications. Specifically, our work lays the foundation for developing efficient quantum transducers for coherent conversion between microwave and optical photons<sup>45</sup>, a crucial step toward interfacing quantum processors with optical communication networks<sup>46</sup>. Additionally, our device has the potential to advance magnon-based quantum memories<sup>44</sup> and enable the integration of storage and transduction functionalities within a single device.

However, due to the relatively low optical quality factor in our current device, we were unable to resolve the mechanical mode in the present generation. This limitation highlights the need for further optimization of the device. Future work will focus on refining the fabrication process and device design to improve optical and mechanical quality factors, as well as to enhance the magnon-phonon and phonon-photon coupling rates. By addressing these challenges, we aim to realize functional optomechanical devices that fulfill the potential envisioned in this work.

#### V. DATA AVAILABILITY

The data that support the findings of this study are available from the corresponding author upon reasonable request.

- <sup>1</sup>M. Aspelmeyer, T. J. Kippenberg, and F. Marquardt, "Cavity optomechanics," *Reviews of Modern Physics* **86** (2014), 10.1103/RevModPhys.86.1391.
- <sup>2</sup>S. Gröblacher, K. Hammerer, M. R. Vanner, and M. Aspelmeyer, "Observation of strong coupling between a micromechanical resonator and an optical cavity field," *Nature* **460** (2009), 10.1038/nature08171.
- <sup>3</sup>S. Barzanjeh, A. Xuereb, S. Gröblacher, M. Paternostro, C. A. Regal, and E. M. Weig, "Optomechanics for quantum technologies," (2022).
- <sup>4</sup>R. A. et al, "Constraints on dark photon dark matter using data from ligo's and virgo's third observing run," *Physical Review D* **105** (2022), 10.1103/PhysRevD.105.063030.
- <sup>5</sup>J. Manley, D. J. Wilson, R. Stump, D. Grin, and S. Singh, "Searching for scalar dark matter with compact mechanical resonators," *Physical Review Letters* **124** (2020), 10.1103/PhysRevLett.124.151301.

- <sup>6</sup>C. G. Baker, W. P. Bowen, P. Cox, M. J. Dolan, M. Goryachev, and G. Harris, "Optomechanical dark matter instrument for direct detection," *Physical Review D* **110** (2024), 10.1103/PhysRevD.110.043005.
- <sup>7</sup>V. Vadakkumbatt, M. Hirschel, J. Manley, T. J. Clark, S. Singh, and J. P. Davis, "Prototype superfluid gravitational wave detector," *Physical Review D* **104** (2021), 10.1103/PhysRevD.104.082001.
- <sup>8</sup>M. Hirschel, V. Vadakkumbatt, N. P. Baker, F. M. Schweizer, J. C. Sankey, S. Singh, and J. P. Davis, "Superfluid helium ultralight dark matter detector," *Physical Review D* **109** (2024), 10.1103/PhysRevD.109.095011.
- <sup>9</sup>P. H. Kim, B. D. Hauer, T. J. Clark, F. F. Sani, M. R. Freeman, and J. P. Davis, "Magnetic actuation and feedback cooling of a cavity optomechanical torque sensor," *Nature Communications* **8** (2017), 10.1038/s41467-017-01380-z.
- <sup>10</sup>M. J. Rudd, P. H. Kim, C. A. Potts, C. Doolin, H. Ramp, B. D. Hauer, and J. P. Davis, "Coherent magneto-optomechanical signal transduction and long-distance phase-shift keying," *Physical Review Applied* **12** (2019), 10.1103/PhysRevApplied.12.034042.
- <sup>11</sup>J. E. Losby, V. T. Sauer, and M. R. Freeman, "Recent advances in mechanical torque studies of small-scale magnetism," (2018).
- <sup>12</sup>W. Jiang, C. J. Sarabalis, Y. D. Dahmani, R. N. Patel, F. M. Mayor, T. P. McKenna, R. V. Laer, and A. H. Safavi-Naeini, "Efficient bidirectional piezo-optomechanical transduction between microwave and optical frequency," *Nature Communications* **11** (2020), 10.1038/s41467-020-14863-3.
- <sup>13</sup>M. Forsch, R. Stockill, A. Wallucks, I. Marinković, C. Gärtner, R. A. Norte, F. van Otten, A. Fiore, K. Srinivasan, and S. Gröblacher, "Microwave-to-optics conversion using a mechanical oscillator in its quantum ground state," *Nature Physics* **16** (2020), 10.1038/s41567-019-0673-7.
- <sup>14</sup>H. Ramp, T. J. Clark, B. D. Hauer, C. Doolin, K. C. Balram, K. Srinivasan, and J. P. Davis, "Wavelength transduction from a 3d microwave cavity to telecom using piezoelectric optomechanical crystals," *Applied Physics Letters* **116** (2020), 10.1063/5.0002160.
- <sup>15</sup>G. Arnold, M. Wulf, S. Barzanjeh, E. S. Redchenko, A. Rueda, W. J. Hease, F. Hassani, and J. M. Fink, "Converting microwave and telecom photons with a silicon photonic nanomechanical interface," *Nature Communications* **11** (2020), 10.1038/s41467-020-18269-z.
- <sup>16</sup>M. J. Weaver, P. Duivesteyn, A. C. Bernasconi, S. Scharmer, M. Lemang, T. C. Thiel, F. Hijazi, B. Hensen, S. Gröblacher, and R. Stockill, "An integrated microwave-to-optics interface for scalable quantum computing," *Nature Nanotechnology* **19** (2024), 10.1038/s41565-023-01515-y.
- <sup>17</sup>B. M. Brubaker, J. M. Kindem, M. D. Urmey, S. Mittal, R. D. Delaney, P. S. Burns, M. R. Vissers, K. W. Lehnert, and C. A. Regal, "Optomechanical ground-state cooling in a continuous and efficient electro-optic transducer," *Physical Review X* **12** (2022), 10.1103/PhysRevX.12.021062.
- <sup>18</sup>A. H. Safavi-Naeini, S. Gröblacher, J. T. Hill, J. Chan, M. Aspelmeyer, and O. Painter, "Squeezed light from a silicon micromechanical resonator," *Nature* **500** (2013), 10.1038/nature12307.
- <sup>19</sup>R. Riedinger, A. Wallucks, I. Marinković, C. Löschnauer, M. Aspelmeyer, S. Hong, and S. Gröblacher, "Remote quantum entanglement between two micromechanical oscillators," in *Nature*, Vol. 556 (2018).
- <sup>20</sup>R. Riedinger, S. Hong, R. A. Norte, J. A. Slater, J. Shang, A. G. Krause, V. Anant, M. Aspelmeyer, and S. Gröblacher, "Non-classical correlations between single photons and phonons from a mechanical oscillator," *Nature* **530** (2016), 10.1038/nature16536.
- <sup>21</sup>S. Hong, R. Riedinger, I. Marinković, A. Wallucks, S. G. Hofer, R. A. Norte, M. Aspelmeyer, and S. Gröblacher, "Hanbury brown and twiss interferometry of single phonons from an optomechanical resonator," *Science* **358** (2017), 10.1126/science.aan7939.
- <sup>22</sup>A. Wallucks, I. Marinković, B. Hensen, R. Stockill, and S. Gröblacher, "A quantum memory at telecom wavelengths," *Nature Physics* **16** (2020), 10.1038/s41567-020-0891-z.
- <sup>23</sup>B. D. Smith, B. Babaei, A. Narayanan, and L. J. LeBlanc, "Microwave-to-optical conversion in a room-temperature 87Rb vapor for frequency-division multiplexing control," *Communications Physics* **6** (2023), 10.1038/s42005-023-01455-y.
- <sup>24</sup>H. T. Tu, K. Y. Liao, Z. X. Zhang, X. H. Liu, S. Y. Zheng, S. Z. Yang, X. D. Zhang, H. Yan, and S. L. Zhu, "High-efficiency coherent microwave-to-optics conversion via off-resonant scattering," *Nature Photonics* **16** (2022), 10.1038/s41566-022-00959-3.

- <sup>25</sup>M. Eichenfield, J. Chan, R. M. Camacho, K. J. Vahala, and O. Painter, "Optomechanical crystals," *Nature* **462**, 78–82 (2009).
- <sup>26</sup>A. H. Safavi-Naeini, J. T. Hill, S. Meenehan, J. Chan, S. Gröblacher, and O. Painter, "Two-dimensional phononic-photonic band gap optomechanical crystal cavity," *Physical Review Letters* **112** (2014), 10.1103/PhysRevLett.112.153603.
- <sup>27</sup>H. Ren, M. H. Matheny, G. S. MacCabe, J. Luo, H. Pfeifer, M. Mirhosseini, and O. Painter, "Two-dimensional optomechanical crystal cavity with high quantum cooperativity," *Nature Communications* **11** (2020), 10.1038/s41467-020-17182-9.
- <sup>28</sup>R. Benevides, F. G. Santos, G. O. Luiz, G. S. Wiederhecker, and T. P. M. Alegre, "Ultra-high-q optomechanical crystal cavities fabricated in a CMOS foundry," *Scientific Reports* **7** (2017), 10.1038/s41598-017-02515-4.
- <sup>29</sup>J. Gomis-Bresco, D. Navarro-Urrios, M. Oudich, S. El-Jallal, A. Griol, D. Puerto, E. Chavez, Y. Pennec, B. Djafari-Rouhani, F. Alzina, A. Martínez, and C. M. Torres, "A one-dimensional optomechanical crystal with a complete phononic band gap," *Nature Communications* **5** (2014), 10.1038/ncomms5452.
- <sup>30</sup>A. H. Safavi-Naeini, T. P. Alegre, J. Chan, M. Eichenfield, M. Winger, Q. Lin, J. T. Hill, D. E. Chang, and O. Painter, "Electromagnetically induced transparency and slow light with optomechanics," *Nature* **472** (2011), 10.1038/nature09933.
- <sup>31</sup>K. E. Grutter, M. Davanco, and K. Srinivasan, "Si<sub>3</sub>N<sub>4</sub> nanobeam optomechanical crystals," *IEEE Journal of Selected Topics in Quantum Electronics* **21** (2015), 10.1109/JSTQE.2014.2376966.
- <sup>32</sup>M. J. Burek, J. D. Cohen, S. M. Meenehan, N. El-Sawah, C. Chia, T. Ruelle, S. Meesala, J. Rochman, H. A. Atikian, M. Markham, D. J. Twitchen, M. D. Lukin, O. Painter, and M. Lončar, "Diamond optomechanical crystals," *Optica* **3** (2016), 10.1364/optica.3.001404.
- <sup>33</sup>X. Zuo, Z. Y. Fan, H. Qian, M. S. Ding, H. Tan, H. Xiong, and J. Li, "Cavity magnomechanics: from classical to quantum," (2024).
- <sup>34</sup>A. A. Serga, A. V. Chumak, and B. Hillebrands, "Yig magnonics," *Journal of Physics D: Applied Physics* **43** (2010), 10.1088/0022-3727/43/26/264002.
- <sup>35</sup>S. Klingler, H. Maier-Flaig, C. Dubs, O. Surzhenko, R. Gross, H. Huebl, S. T. Goennenwein, and M. Weiler, "Gilbert damping of magnetostatic modes in a yttrium iron garnet sphere," *Applied Physics Letters* **110** (2017), 10.1063/1.4977423.
- <sup>36</sup>S. H. Wemple, S. L. Blank, J. A. Seman, and W. A. Biolsi, "Optical properties of epitaxial iron garnet thin films," *Physical Review B* **9** (1974), 10.1103/PhysRevB.9.2134.
- <sup>37</sup>C. A. Potts, V. A. Bittencourt, S. V. Kusminskiy, S. V. Kusminskiy, and J. P. Davis, "Magnon-phonon quantum correlation thermometry," *Physical Review Applied* **13** (2020), 10.1103/PhysRevApplied.13.064001.
- <sup>38</sup>C. A. Potts, Y. Huang, V. A. Bittencourt, S. V. Kusminskiy, and J. P. Davis, "Dynamical backaction evading magnomechanics," *Physical Review B* **107** (2023), 10.1103/PhysRevB.107.L140405.
- <sup>39</sup>V. A. Bittencourt, C. A. Potts, Y. Huang, J. P. Davis, and S. V. Kusminskiy, "Magnomechanical backaction corrections due to coupling to higher-order walker modes and Kerr nonlinearities," *Physical Review B* **107** (2023), 10.1103/PhysRevB.107.144411.
- <sup>40</sup>Z. X. Liu, J. Peng, and H. Xiong, "Generation of magnonic frequency combs via a two-tone microwave drive," *Physical Review A* **107** (2023), 10.1103/PhysRevA.107.053708.
- <sup>41</sup>J. Li, Y. P. Wang, W. J. Wu, S. Y. Zhu, and J. Q. You, "Quantum network with magnonic and mechanical nodes," *PRX Quantum* **2** (2021), 10.1103/PRXQuantum.2.040344.
- <sup>42</sup>X. Zhang, N. Zhu, C. L. Zou, and H. X. Tang, "Optomagnonic whispering gallery microresonators," *Physical Review Letters* **117** (2016), 10.1103/PhysRevLett.117.123605.
- <sup>43</sup>X. Zhang, C. L. Zou, L. Jiang, and H. X. Tang, "Strongly coupled magnons and cavity microwave photons," *Physical Review Letters* **113** (2014), 10.1103/PhysRevLett.113.156401.
- <sup>44</sup>X. Zhang, C. L. Zou, N. Zhu, F. Marquardt, L. Jiang, and H. X. Tang, "Magnon dark modes and gradient memory," *Nature Communications* **6** (2015), 10.1038/ncomms9914.
- <sup>45</sup>F. Engelhardt, V. A. Bittencourt, H. Huebl, O. Klein, and S. V. Kusminskiy, "Optimal broadband frequency conversion via a magnetomechanical transducer," *Physical Review Applied* **18** (2022), 10.1103/PhysRevApplied.18.044059.
- <sup>46</sup>C. Simon, "Towards a global quantum network," *Nature Photonics* **11** (2017), 10.1038/s41566-017-0032-0.
- <sup>47</sup>N. Zhu, X. Zhang, X. Han, C. L. Zou, and H. X. Tang, "Inverse Faraday effect in an optomagnonic waveguide," *Physical Review Applied* **18** (2022), 10.1103/PhysRevApplied.18.024046.
- <sup>48</sup>P. Trempler, R. Dreyer, P. Geyer, C. Hauser, G. Woltersdorf, and G. Schmidt, "Integration and characterization of micron-sized yig structures with very low Gilbert damping on arbitrary substrates," *Applied Physics Letters* **117** (2020), 10.1063/5.0026120.
- <sup>49</sup>G. Schmidt, C. Hauser, P. Trempler, M. Paleschke, and E. T. Papaioannou, "Ultra thin films of yttrium iron garnet with very low damping: A review," *Physica Status Solidi (B) Basic Research* **257** (2020), 10.1002/pssb.201900644.
- <sup>50</sup>H. Arisawa, S. Daimon, Y. Oikawa, Y. J. Seo, K. Harii, K. Oyanagi, and E. Saitoh, "Magnetomechanical sensing based on delta-e effect in y<sub>3</sub>fe<sub>5</sub>o<sub>12</sub> micro bridge," *Applied Physics Letters* **114** (2019), 10.1063/1.5090272.
- <sup>51</sup>N. Zhu, H. Chang, A. Franson, T. Liu, X. Zhang, E. Johnston-Halperin, M. Wu, and H. X. Tang, "Patterned growth of crystalline y<sub>3</sub>fe<sub>5</sub>o<sub>12</sub> nanostructures with engineered magnetic shape anisotropy," *Applied Physics Letters* **110** (2017), 10.1063/1.4986474.
- <sup>52</sup>F. Heyroth, C. Hauser, P. Trempler, P. Geyer, F. Syrowatka, R. Dreyer, S. G. Ebbinghaus, G. Woltersdorf, and G. Schmidt, "Monocrystalline freestanding three-dimensional yttrium-iron-garnet magnon nanoresonators," *Physical Review Applied* **12** (2019), 10.1103/PhysRevApplied.12.054031.
- <sup>53</sup>COMSOL *Multiphysics® v. 6.0.*, COMSOL AB, Stockholm, Sweden (2023).
- <sup>54</sup>C. S. Kim, S. H. Ahn, and D. Y. Jang, "Review: Developments in micro/nanoscale fabrication by focused ion beams," (2012).
- <sup>55</sup>S. Khizroev and D. Litvinov, "Focused-ion-beam-based rapid prototyping of nanoscale magnetic devices," (2004).
- <sup>56</sup>A. E. Fraser, *Focused Ion Beam Milled Magnetic Cantilevers*, Ph.D. thesis, University of Alberta, Edmonton, Canada (2010).
- <sup>57</sup>J. E. Losby, F. F. Sani, D. T. Grandmont, Z. Diao, M. Belov, J. A. Burgess, S. R. Compton, W. K. Hiebert, D. Vick, K. Mohammad, E. Salimi, G. E. Bridges, D. J. Thomson, and M. R. Freeman, "Torque-mixing magnetic resonance spectroscopy," *Science* **350** (2015), 10.1126/science.aad2449.
- <sup>58</sup>G. A. Horridge and S. L. Tamm, "Critical point drying for scanning electron microscopic study of ciliary motion," *Science* **163** (1969), 10.1126/science.163.3869.817.
- <sup>59</sup>B. D. Hauer, P. H. Kim, C. Doolin, A. J. MacDonald, H. Ramp, and J. P. Davis, "On-chip cavity optomechanical coupling," *EPJ Techniques and Instrumentation* **1** (2014), 10.1140/epjti4.
- <sup>60</sup>H. Kerdoncuff, U. B. Hoff, G. I. Harris, W. P. Bowen, and U. L. Andersen, "Squeezing-enhanced measurement sensitivity in a cavity optomechanical system," *Annalen der Physik* **527** (2015), 10.1002/andp.201400171.
- <sup>61</sup>J. Chan, A. H. Safavi-Naeini, J. T. Hill, S. Meenehan, and O. Painter, "Optimized optomechanical crystal cavity with acoustic radiation shield," *Applied Physics Letters* **101** (2012), 10.1063/1.4747726.
- <sup>62</sup>R. W. Dixon and H. Matthews, "Diffraction of light by elastic waves in yig," *Applied Physics Letters* **10** (1967), 10.1063/1.1754907.
- <sup>63</sup>R. T. Lynch, J. F. Dillon, and L. G. V. Uitert, "Stress birefringence in ferrimagnetic garnets," *Journal of Applied Physics* **44** (1973), 10.1063/1.1661866.
- <sup>64</sup>Y. Li, K. Cui, X. Feng, Y. Huang, Z. Huang, F. Liu, and W. Zhang, "Optomechanical crystal nanobeam cavity with high optomechanical coupling rate," *Journal of Optics (United Kingdom)* **17** (2015), 10.1088/2040-8978/17/4/045001.
- <sup>65</sup>M. Eichenfield, R. Camacho, J. Chan, K. J. Vahala, and O. Painter, "A picogram- and nanometre-scale photonic-crystal optomechanical cavity," *Nature* **459** (2009), 10.1038/nature08061.
- <sup>66</sup>J. Chan, M. Eichenfield, R. Camacho, and O. Painter, "Optical and mechanical design of a "zipper" photonic crystal optomechanical cavity," in *Optics InfoBase Conference Papers* (2009).
- <sup>67</sup>R. Leijssen and E. Verhagen, "Strong optomechanical interactions in a sliced photonic crystal nanobeam," *Scientific Reports* **5** (2015), 10.1038/srep15974.
- <sup>68</sup>J. Graf, S. Sharma, H. Huebl, and S. V. Kusminskiy, "Design of an optomagnonic crystal: Towards optimal magnon-photon mode matching at the microscale," *Physical Review Research* **3** (2021), 10.1103/PhysRevResearch.3.013277.

<sup>69</sup>G. Venkat, D. Kumar, M. Franchin, O. Dmytriiev, M. Mruczkiewicz, H. Fangohr, A. Barman, M. Krawczyk, and A. Prabhakar, "Proposal for a standard micromagnetic problem: Spin wave dispersion in a magnonic waveguide," *IEEE Transactions on Magnetics* **49** (2013), 10.1109/TMAG.2012.2206820.

<sup>70</sup>A. Vansteenkiste, J. Leliaert, M. Dvornik, M. Helsen, F. Garcia-Sanchez, and B. V. Waeyenberge, "The design and verification of mumax3," *AIP Advances* **4** (2014), 10.1063/1.4899186.